

Theoretical Study of the Kinetics of the Reactions $\text{Se} + \text{O}_2 \rightarrow \text{SeO} + \text{O}$ and $\text{As} + \text{HCl} \rightarrow \text{AsCl} + \text{H}$

David R. Urban and Jennifer Wilcox*

Department of Chemical Engineering, Worcester Polytechnic Institute, 100 Institute Road, Worcester, Massachusetts 01609

Received: May 11, 2006; In Final Form: May 18, 2006

Selenium and arsenic reactions believed to take place in the flue gases of coal combustion facilities were investigated. Prior theoretical work involving various As and Se species was completed using DFT and a broad range of ab initio methods. Building upon that work, the present study is a determination of the kinetic and thermodynamic parameters of the reactions, $\text{Se} + \text{O}_2 \rightarrow \text{SeO} + \text{O}$ and $\text{As} + \text{HCl} \rightarrow \text{AsCl} + \text{H}$ at the CCSD/RCEP28VDZ and QCISD(T)/6-311++G(3df,3pd) levels of theory, respectively. Transition state theory was used in determining the kinetic rate constants along with collision theory as a means of comparison. The calculated K_{eq} values are compared to experimental data, where available.

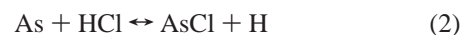
Introduction

As environmental regulations pertaining to mercury are becoming much stricter, other trace metals, particularly arsenic and selenium, are beginning to be examined as well. A noted source of compounds containing these elements is coal combustion flue gases and, as such, the mechanism(s) of their removal is a topic of much attention.^{1,2} Given that any removal strategy will be dependent upon the speciation, and the speciation in turn will be dependent upon the reaction kinetics of the flue gas, determination of the kinetic parameters of reactions involving these metals is key to developing effective removal techniques.

Previous experimental work has been performed to determine the speciation for a variety of conditions with numerous studies^{3–5} having found selenium oxide compounds to be the dominant Se species at high temperatures (>1500 K) and AsCl_3 to be predominant at midrange temperatures (800–1200 K). Unfortunately, the nature of many of the intermediate compounds created as a result of the combustion process makes them undetectable to current experimental techniques. To develop a more complete understanding of the overall speciation, it is thus necessary to determine the importance of these compounds. To accomplish this, computational chemistry techniques are employed to determine the kinetic parameters of the elementary reactions taking place within the combustion flue gas environment.

Although selenium oxides and arsenic chlorides are thought to be major components of the flue gas, in particular SeO_2 and AsCl_3 , the mechanisms for their formation may follow several paths. It is possible that they are released as is from the solid coal matrix; however, it is also possible that As and Se are released from the coal in elemental form and so the ultimate speciation is a product of several elementary steps. As oxygen would be in excess in a typical combustion process, the formation of selenium oxides is natural. Because some forms of coal contain little chlorine, the reaction of As with HCl is not as common; but in systems for which chlorine is present

up to 99% of the chlorine has been found to be in the form of HCl, making this reaction very important for coals with chlorinated compounds.³ Knowing this, the following bimolecular formation reactions of the single-constituent compounds (SeO , AsCl) were selected for study:



Because these reactions are both single displacement reactions, transition state theory (TST) was used to determine the kinetic parameters of forward and reverse reactions for a temperature range of 298.15–2000 K at atmospheric pressure. Additionally, the hard sphere collision model was used to calculate the rate constant, setting an upper-bound from which the values obtained from TST fall approximately 2 orders of magnitude below.

Computational Methodology

Calculations were carried out using the Gaussian 03 suite of programs.⁶ Basis sets incorporating relativistic effects were employed through the use of small core relativistic effective core potentials (RECP) for the inner electrons of arsenic and selenium. A relativistic compact effective potential, RECP28VDZ of the Stevens et al. group,⁷ which replaces 28 of arsenic's and 28 of selenium's atomic core electrons, derived from numerical Dirac–Fock wave functions using an optimizing process based upon the energy-overlap functional was employed. Energy-optimized (5s5p)/[2s2p] Gaussian type double- ζ quality sp and triple- ζ quality d functions were used, with the triple- ζ d functions essential for describing the orbital shape changes that exist with d occupancy. To compare the theoretical predictions from the pseudopotentials to those of a complete basis set, calculations were performed using the 6-311++G(3pd,3df) Pople basis set for the smaller arsenic and selenium containing compounds. Additionally, this extended Pople basis set, which includes both diffuse and polarization functions, was used for hydrogen, oxygen, and chlorine.

Before the kinetic and equilibrium parameters could be calculated, it was necessary to determine which level of theory

* Corresponding author. Tel: 508-831-5493. Fax: 508-831-5853. E-mail: jwilcox@wpi.edu.

TABLE 1: Theory Selection Criteria Comparison

parameter	CCSD/RECP28VDZ	exp ^{14,15}	parameter	QCISD(T)/6-311++G(3df,3pd)	exp ^{14,15}
bond length (Å) SeO	1.6718	1.6393	bond length (Å) AsCl	2.1604	
vib freq (cm ⁻¹) SeO	848.38	914.69	Vib freq (cm ⁻¹) AsCl	425.58	424
ΔH _{R1} (kcal/mol)	17.64	18.20	ΔH _{R2} (kcal/mol)	34.87	29.87

would be most accurate for each reaction. The process for theory selection has been previously detailed⁸ and so will not be discussed in detail here; suffice it to say that the level of theory chosen for reaction 1 was CCSD/RECP28VDZ and that for reaction 2 was QCISD(T)/6-311++G(3df,3pd) after comparison with a number of combinations of methods and basis sets. The data of the relevant parameters at the reaction level of theory and from experiment are given in Table 1. From this information, the deviation in reaction enthalpy is seen to be 0.56 and 5.01 kcal/mol for reactions 1 and 2, respectively, whereas the deviations in the primary species are 0.03 Å and 66.31 cm⁻¹ for the bond length and vibrational frequency of SeO, and 1.58 cm⁻¹ for the vibrational frequency of AsCl. It is important to note that the frequency calculated for AsCl is based upon a geometry optimized at the lower QCISD/6-311++G(3df,3pd) level of theory.

Theoretical Kinetic Methodology

Kinetic and equilibrium parameters were evaluated over a temperature range spanning 298.15–2000 K. In determining the rate constant for each reaction, the transition state theory (3)⁹ was modified with the tunneling correction factor of Wigner¹⁰ (4) (where ν represents the single imaginary frequency value of the transition structure), so that the final rate constant value was given by (5).

$$k^{\text{TST}} = \frac{k_b T}{h} \frac{Q_{\text{TS}}}{Q_1 Q_2} e^{-E_a/RT} \quad (3)$$

$$k_T = 1 + \frac{1}{24} \left[\frac{h c \nu}{k_b T} \right]^2 \quad (4)$$

$$k = k^{\text{TST}} k_T \quad (5)$$

The calculation of the rate constant based on the hard sphere collision model was performed using eq 6 taken from Steinfeld.¹¹ Because collision theory assumes all collisions produce reactions, it provides an upper-bound value for the subsequent calculation using TST; finding a TST value greater than that of the hard sphere collision model is an instant confirmation of some error.

$$k^{\text{Coll}} = \pi \sigma_{12}^2 N_A \sqrt{\frac{8k_b T}{\pi \mu_{12}}} e^{-E_a/RT} \frac{\text{cm}^3}{\text{mol} \cdot \text{s}} \quad (6)$$

where the activation energy is the same as for k^{TST} , μ_{12} is the reduced mass in g/particle, and σ_{12} is the collision diameter in Å. Because E_a is already known, and μ can be determined with a simple calculation, the only difficulty was in determining the collision diameter. Here, the lack of experimental data required the use of estimation techniques to find an approximate value of σ . The primary technique utilized was a traditional approach based upon the critical properties of the species in the reaction as shown in

$$\sigma = 0.1866 V_c^{1/3} Z_c^{-6/5} \text{ Å} \quad (7)$$

The value of σ_{12} is then the average of the σ values for both

species. Because this method requires knowledge of all critical parameters (T_c and P_c are used in calculating Z_c), it was not always practical to use due to the limited information on the critical parameters for some arsenic- and selenium-containing compounds; in these instances the collision diameter was determined by evaluating the value of σ for each atom and taking the sum. The σ for both elemental As and Se could be found from the critical parameters and the values for H, Cl, and O were found by dividing the σ of the diatomics H₂, Cl₂, and O₂ in half. In this way a crude estimate of the collision diameter was determined for those compounds for which no experimental σ or critical parameters existed.

Additionally, the equilibrium constants for each reaction were calculated from eqs 8 and 9. By determination of the thermodynamic parameters of reaction enthalpy and entropy, the

$$K_{\text{eq}} = e^{-\Delta G/RT} \quad (8)$$

$$\Delta G = \Delta H - T\Delta S \quad (9)$$

equilibrium curve as predicted both theoretically and experimentally could be compared, where all data existed. In this way, an evaluation could be made of these quantities as well as the ratio of the rate constants to determine if the theoretical predictions, both kinetic and thermodynamic, matched existing experimental thermodynamic data.

Results and Discussion

A. Formation of Selenium Monoxide. Figure 1 shows the potential energy surface of reaction 1. It should be noted that to present the 3-dimensional surface, one degree of freedom had to be restricted; in this case the transition structure was assumed to be linear, thus the two variables were the O–O and the O–Se bond distances. As can be seen in Figure 1, a saddle point appears at approximately (1.53 Å, 1.90 Å) on the surface and it was this value that was found to possess the one imaginary frequency indicative of a transition structure; the relevant parameters of this transition structure are given in Table 2. Having identified the transition structure for this reaction, the

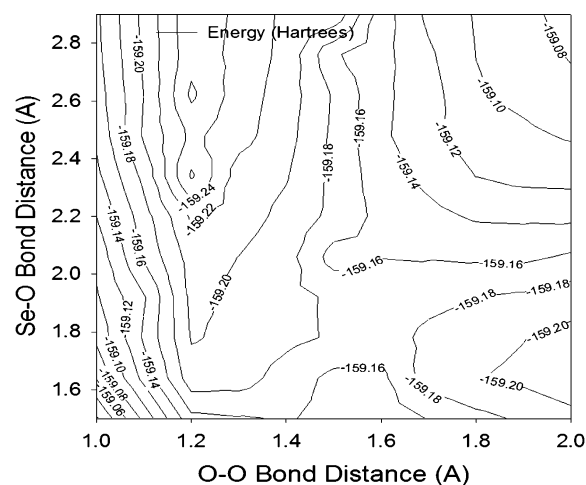


Figure 1. Se + O₂ → SeO + O: linear transition structure (CCSD/RECP28VDZ).

TABLE 2: Transition Structure Parameters

	SeOO	AsClH
bond length (Å) Se–O; As–Cl	1.90	2.25
bond length (Å) O–O; Cl–H	1.53	1.85
bond angle (deg)	180.0	180.0
vibrational frequencies (cm^{-1})	213.51	279.18
	230.84	280.29
	418.02	399.77
	1229.46i	894.20i
single point energy (hartrees)	–159.17	–2694.51
spin multiplicity	5	4
rotational constant (GHZ)	2.786	3.815
I_{xx} ($\text{amu}\cdot\text{Å}^2$)	0	0
I_{yy} ($\text{amu}\cdot\text{Å}^2$)	180.45	133.22
I_{zz} ($\text{amu}\cdot\text{Å}^2$)	180.45	133.22

kinetic rate parameters were then investigated using transition state theory and the hard sphere collision model. The natural log of the forward rate constant [$\text{cm}^3/\text{mol}/\text{s}$] as a function of the inverse of temperature (K) is given for both methods in Figure 2. Evaluating the trendlines associated with each method shows that, over the given temperature range, the Arrhenius expressions are

$$k_f^{\text{TST}} = 2.32 \times 10^{13} e^{-55.15/RT} \frac{\text{cm}^3}{\text{mol}\cdot\text{s}} \quad (10)$$

$$k_f^{\text{Coll}} = 1.55 \times 10^{14} e^{-54.49/RT} \frac{\text{cm}^3}{\text{mol}\cdot\text{s}} < \quad (11)$$

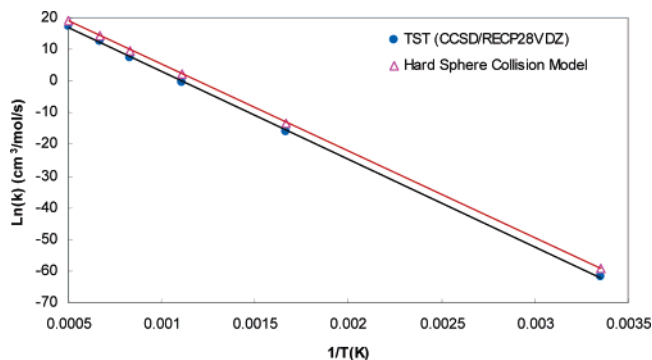
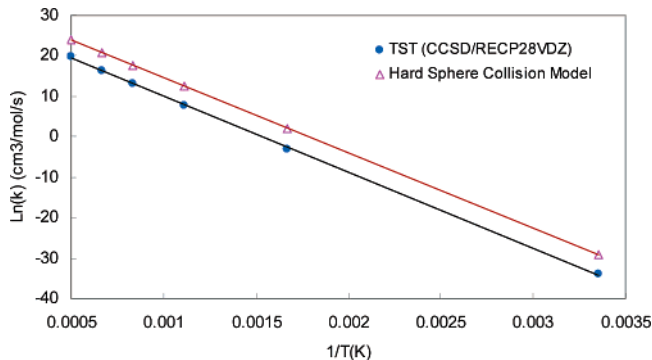
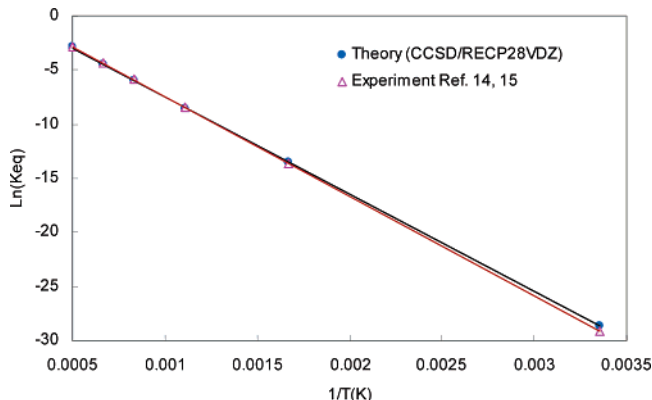
The kinetic parameters of the reverse reaction are plotted in Figure 3. Applying the same evaluation, the Arrhenius expressions are

$$k_r^{\text{TST}} = 3.32 \times 10^{12} e^{-37.39/RT} \frac{\text{cm}^3}{\text{mol}\cdot\text{s}} \quad (12)$$

$$k_r^{\text{Coll}} = 2.71 \times 10^{14} e^{-37.02/RT} \frac{\text{cm}^3}{\text{mol}\cdot\text{s}} \quad (13)$$

Again the frequency factor found using transition state theory is several orders of magnitude below that predicted for the collision model. Evaluation of the tunneling correction factor showed that it increased the rate constant by 2.5 times, for both forward and reverse reactions, at ambient conditions but the impact decreased dramatically and at a 600 K the increase was only a factor of 1.4; at still higher temperatures the correction is essentially negligible. Also, the activation energies used in the rate constant equations were compared to the exact values at each temperature and it was found that the forward reaction activation energy of 55.15 kcal/mol (from TST) deviated by no more than 2.02 kcal/mol whereas the reverse reaction value of 37.39 kcal/mol deviated at most by 1.34 kcal/mol. These highest deviations were found at the maximum temperature examined, 2000 K, suggesting that the deviation from the developed model will increase as the temperature is elevated.

Additionally, the thermodynamic properties for this reaction were calculated from theory and compared to available experimental data, as seen in Figure 4. It should be noted that the experimental thermodynamic values were obtained from Chase¹² (O and O₂) and Barin¹³ (Se and SeO). From this plot, the parameters over the entire temperature range are $\Delta H_{\text{rxn}}^{\text{Th}} = 17.87$ kcal/mol, $\Delta S_{\text{rxn}}^{\text{Th}} = 3.05$ (cal/mol)/K, $\Delta H_{\text{rxn}}^{\text{Exp}} = 18.32$ kcal/mol, and $\Delta S_{\text{rxn}}^{\text{Exp}} = 3.55$ (cal/mol)/K. This information was used to calculate the equilibrium constant for the reaction.

**Figure 2.** Rate constant as a function of temperature ($\text{Se} + \text{O}_2 \rightarrow \text{SeO} + \text{O}$).**Figure 3.** Rate constant as a function of temperature ($\text{SeO} + \text{O} \rightarrow \text{Se} + \text{O}_2$).**Figure 4.** Equilibrium constant as a function of temperature ($\text{SeO} + \text{O} \rightarrow \text{Se} + \text{O}_2$).

B. Formation of Arsenic Monochloride. The same basic procedure was followed in the determination of the kinetic and thermodynamic parameters of reaction 2. Figure 5 shows the potential energy surface of the particular transition compound formed in this reaction. Here, again, the saddle point is clearly illustrated and the approximate coordinates (1.85 Å, 2.25 Å) proved to be a true transition structure with a single imaginary frequency; as before, the parameters are shown in Table 2. Once again, the linearity assumption was made to allow for a three-dimensional surface plot. Using the same procedure as with the selenium reaction, the kinetic parameters of this reaction were determined as well. Figures 6 and 7 illustrate the rate constant of the forward and reverse reaction, respectively. The impact of tunneling was less pronounced in this reaction with the rate constant of both forward and reverse reactions being increased by a factor of 1.8 at ambient temperatures and only 1.2 at 600 K; again, at higher temperatures the correction factor is essentially 1.0. Comparison of the TST activation energies

TABLE 3: Kinetic and Thermodynamic Parameters ($\text{Se} + \text{O}_2 \rightarrow \text{SeO} + \text{O}$)

parameter	temp (K)					
	298.15	600	900	1200	1500	2000
k_f [(cm ³ /mol)/s]	8.721×10^{-28}	1.894×10^{-7}	0.940	2.095×10^3	2.138×10^5	2.181×10^7
k_r [(cm ³ /mol)/s]	1.289×10^{-15}	7.947×10^{-2}	2.758×10^3	5.137×10^5	1.182×10^7	2.722×10^8
k_f/k_r	6.77×10^{-13}	2.38×10^{-6}	3.41×10^{-4}	4.08×10^{-3}	1.81×10^{-2}	8.01×10^{-2}
$K_{\text{eq}}(\text{th})$	3.69×10^{-13}	1.44×10^{-6}	2.12×10^{-4}	2.58×10^{-3}	1.15×10^{-2}	5.17×10^{-2}
$K_{\text{eq}}(\text{exp})$	2.21×10^{-13}	1.26×10^{-6}	2.12×10^{-4}	2.74×10^{-3}	1.28×10^{-2}	5.93×10^{-2}

TABLE 4: Kinetic and Thermodynamic Parameters ($\text{As} + \text{HCl} \rightarrow \text{AsCl} + \text{H}$)

parameter	temp (K)					
	298.15	600	900	1200	1500	2000
k_f [(cm ³ /mol)/s]	3.261×10^{-17}	4.087×10^{-2}	3.823×10^3	1.169×10^6	3.624×10^7	1.123×10^9
k_r [(cm ³ /mol)/s]	1.342×10^9	1.797×10^{11}	9.013×10^{11}	2.018×10^{12}	3.274×10^{12}	5.311×10^{12}
k_f/k_r	2.43×10^{-26}	2.27×10^{-13}	4.24×10^{-9}	5.79×10^{-7}	1.11×10^{-5}	2.12×10^{-4}
$K_{\text{eq}}(\text{th})$	3.34×10^{-26}	3.76×10^{-13}	7.44×10^{-9}	1.05×10^{-6}	2.04×10^{-5}	3.97×10^{-4}
$K_{\text{eq}}(\text{exp})$						

shows that the forward reaction value of 40.94 kcal/mol deviated by 2.81 kcal/mol whereas the reverse reaction value of 5.77 kcal/mol was off by only 1.00 kcal/mol, again, both reaching the maximum deviation at 2000 K. Unfortunately, no experimental thermodynamic data could be found for AsCl and so no equilibrium constant comparison could be made; however, the parameters derived from theory were found to be $\Delta H_{\text{rxn}}^{\text{Th}} = 35.39$ kcal/mol, $\Delta S_{\text{rxn}}^{\text{Th}} = 2.13$ (cal/mol)/K. The following equations summarize the data generated from the kinetic plots:

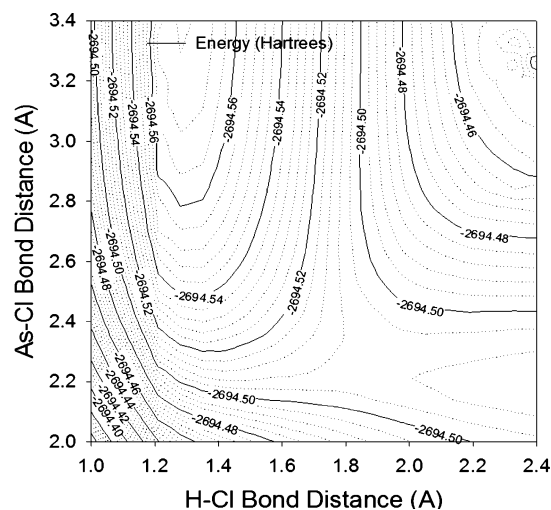
$$k_f^{\text{TST}} = 3.35 \times 10^{13} e^{-40.94/RT} \frac{\text{cm}^3}{\text{mol}\cdot\text{s}} \quad (14)$$

$$k_f^{\text{Coll}} = 1.12 \times 10^{15} e^{-40.03/RT} \frac{\text{cm}^3}{\text{mol}\cdot\text{s}} \quad (15)$$

$$k_r^{\text{TST}} = 2.27 \times 10^{13} e^{-5.77/RT} \frac{\text{cm}^3}{\text{mol}\cdot\text{s}} \quad (16)$$

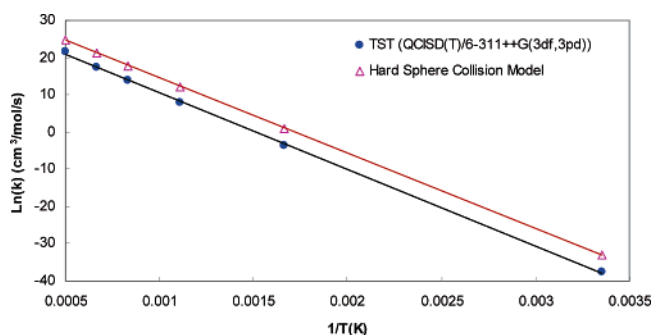
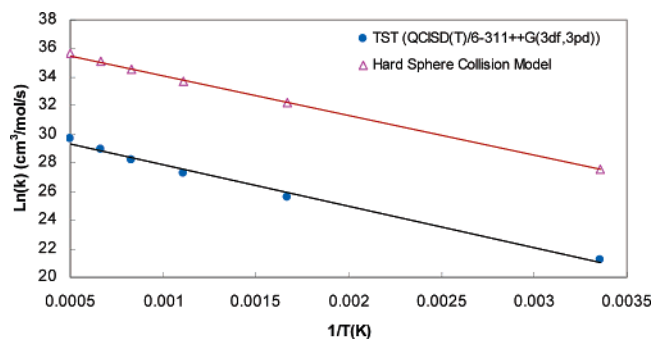
$$k_r^{\text{Coll}} = 1.08 \times 10^{16} e^{-5.56/RT} \frac{\text{cm}^3}{\text{mol}\cdot\text{s}} \quad (17)$$

C. Data Comparison. One final aspect of these reactions that should be considered is how the speciation predicted by the calculated parameters compares to existing experimental data. Tables 3 and 4 present the theoretical and experimental values of k_f , k_r , and K_{eq} for reactions 1 and 2, respectively, over

**Figure 5.** $\text{As} + \text{HCl} \rightarrow \text{AsCl} + \text{H}$: linear transition structure (QCISD(T)/6-311++G(3df,3pd)).

the entire range of temperatures examined. For both reactions, the value of k_f/k_r is of the same order of magnitude as that for K_{eq} and for reaction 1 they are both comparable to the experimental equilibrium curve. The fact that the theoretical calculations of the kinetics and thermodynamics, having been determined using completely separate approaches, support each other in both reactions, and in the case of reaction 1 are supported by experiment, serves as a further validation of their accuracy. Unfortunately, no experimental kinetics data are available for additional comparison.

The experimental speciation studies conducted have all been based upon an equilibrium model. Yan³ predicted that, under oxidizing conditions and in the presence of chlorine, SeO would be the predominant Se species at temperatures above 1500 K but, under reducing conditions, it would not be a major flue gas constituent at any temperature. In a later experiment, Yan⁵ found that, in Se-impregnated coke/coal, SeO was the dominant species above 600 K under oxidizing conditions and was a minor Se constituent above 1100 K under reducing conditions. The

**Figure 6.** Rate constant as a function of temperature ($\text{As} + \text{HCl} \rightarrow \text{AsCl} + \text{H}$).**Figure 7.** Rate constant as a function of temperature ($\text{AsCl} + \text{H} \rightarrow \text{As} + \text{HCl}$).

K_{eq} data in Table 3 show that the formation of SeO through this particular reaction pathway is not favored at any temperature examined. This suggests that there must be one or more additional reaction channels that lead to the creation of SeO.

Unfortunately, the radical species AsCl was not found in any experimental studies, most likely a consequence of its short lifespan in the flue gas. It is suspected that it is a link in the chain of reactions leading to the formation of AsCl_3 , a major constituent species at intermediate temperatures 600–1400 K, as determined by Yan.³ What can be determined from the present study, is that the AsCl formation reaction examined is most likely not a major contributor to the overall AsCl formation, given that the K_{eq} values provided in Table 4 show that the creation of elemental As is favored over AsCl over the entire temperature range.

Conclusions

With the increase in emphasis upon selenium and arsenic compounds in the field of coal combustion, the kinetic data calculated here represent the first step in the effort to design effective removal methods for the most harmful species. It is unfortunate that, owing to the difficulty of measurement, there are no experimental kinetic data available to compare to the theory; however, this only further stresses the need for computational chemistry modeling in this area. Additionally, the nearly identical theoretical and experimental equilibrium plots for reaction 1 provide further evidence of the accuracy of these theoretical predictions.

Ultimately, this same process will be repeated with many different, yet similar, reactions. The complete network of mechanisms leading to the formation of SeO_2 , AsCl_3 , and other arsenic and selenium species known to be present in the flue gas, will need to be studied; the overall goal being the development of a comprehensive flue gas model capable of predicting the speciation of these trace metals under a variety of process conditions.

Acknowledgment. Some of the high-level computations were performed through the Center for Computational Science and the Scientific Computing and Visualization Group at Boston University, which is partners with NSF and sponsored by the National Computational Science Alliance at Boston University. This material is based upon work supported by the National Science Foundation under Grant No. 0448758.

References and Notes

- (1) Diaz-Somoano, M.; Martinez-Tarazona, M. R. Retention of Arsenic and Selenium Compounds Using Limestone in a Coal Gasification Flue Gas. *Environ. Sci. Technol.* **2004**, *38*, 899–903.
- (2) Agnihotri, R.; Chauk, S.; Mahuli, S.; Fan, L.-S. Selenium Removal Using Ca-Based Sorbents: Reaction Kinetics. *Environ. Sci. Technol.* **1998**, *32*, 1841–1846.
- (3) Yan, R.; Gauthier, D.; Flamant, G. Possible Interactions Between As, Se, and Hg During Coal Combustion. *Combust. Flame* **2000**, *120*, 49–60.
- (4) Andren, A. W.; Klein, D. H. Selenium in Coal-Fired Steam Plant Emissions. *Environ. Sci. Technol.* **1975**, *9* (9), 856–858.
- (5) Yan, R.; Gauthier, D.; Flamant, G.; Peraudeau, G. Fate of Selenium in Coal Combustion: Volatilization and Speciation in the Flue Gas. *Environ. Sci. Technol.* **2001**, *35* (7), 1406–1410.
- (6) Frisch, M. J.; Trucks, G. W.; Schlegel, H. B.; Scuseria, G. E.; Robb, M. A.; Cheeseman, J. R.; Montgomery, J. A., Jr.; Vreven, T.; Kudin, K. N.; Burant, J. C.; Millam, J. M.; Iyengar, S. S.; Tomasi, J.; Barone, V.; Mennucci, B.; Cossi, M.; Scalmani, G.; Rega, N.; Petersson, G. A.; Nakatsuji, H.; Hada, M.; Ehara, M.; Toyota, K.; Fukuda, R.; Hasegawa, J.; Ishida, M.; Nakajima, T.; Honda, Y.; Kitao, O.; Nakai, H.; Klene, M.; Li, X.; Knox, J. E.; Hratchian, H. P.; Cross, J. B.; Bakken, V.; Adamo, C.; Jaramillo, J.; Gomperts, R.; Stratmann, R. E.; Yazyev, O.; Austin, A. J.; Cammi, R.; Pomelli, C.; Ochterski, J. W.; Ayala, P. Y.; Morokuma, K.; Voth, G. A.; Salvador, P.; Dannenberg, J. J.; Zakrzewski, V. G.; Dapprich, S.; Daniels, A. D.; Strain, M. C.; Farkas, O.; Malick, D. K.; Rabuck, A. D.; Raghavachari, K.; Foresman, J. B.; Ortiz, J. V.; Cui, Q.; Baboul, A. G.; Clifford, S.; Cioslowski, J.; Stefanov, B. B.; Liu, G.; Liashenko, A.; Piskorz, P.; Komaromi, I.; Martin, R. L.; Fox, D. J.; Keith, T.; Al-Laham, M. A.; Peng, C. Y.; Nanayakkara, A.; Challacombe, M.; Gill, P. M. W.; Johnson, B.; Chen, W.; Wong, M. W.; Gonzalez, C.; and Pople, J. A. *Gaussian 03*, revision C.02; Gaussian, Inc.: Wallingford, CT, 2004.
- (7) Stevens, W. J.; Krauss, M. Relativistic compact effective core potentials and efficient, shared-exponent basis sets for the third-, fourth-, and fifth-row atoms. *Can. J. Chem.* **1992**, *70*, 612–630.
- (8) Urban, D. R.; Wilcox, J. A Theoretical Study of Properties and Reactions Involving arsenic and Selenium Compounds Present in Coal Combustion Flue Gases. *J. Phys. Chem. A*, in press.
- (9) Eyring, H. The activated complex in chemical reactions. *J. Chem. Phys.* **1935**, *3*, 107.
- (10) Wigner, E. Crossing of potential thresholds in chemical reactions. *Z. Phys. Chem. B* **1932**, *19*, 203.
- (11) Steinfeld, J. I.; Francisco, J. S.; Hase, W. L. *Chemical Kinetics and Dynamics*, 2nd ed.; Prentice Hall: Upper Saddle River, NJ, 1999.
- (12) Chase, M. W., Jr. NIST-JANAF Thermochemical Tables, 4th ed. *J. Phys. Chem. Ref. Data* **1998**, Monograph 9, 1–1951
- (13) Barin, I.; Knacke, O.; Kubaschewski, O. *Thermochemical properties of inorganic substances. Supplement*; Springer-Verlag: Berlin, 1977; p 861.
- (14) Thermodynamics Research Center, NIST Boulder Laboratories, M. Frenkel director. Thermodynamics Source Database. In *NIST Chemistry WebBook*; NIST Standard Reference Database Number 69; Linstrom, P. J., Mallard, W. G., Eds.; National Institute of Standards and Technology: Gaithersburg, MD, 20899; June 2005 (<http://webbook.nist.gov>).
- (15) Lide, D. R. *CRC Handbook of Chemistry and Physics*; CRC Press: Boca Raton, FL, 2005.